

Attention-Aided MMSE for OFDM Channel Estimation: Learning Linear Filters with Attention

TaeJun Ha, Chaehyun Jung, Hyeonuk Kim, Jeongwoo Park, and Jeonghun Park

Abstract—In orthogonal frequency division multiplexing (OFDM), accurate channel estimation is crucial. Classical signal processing-based approaches, such as linear minimum mean-squared error (LMMSE) estimation, often require second-order statistics that are difficult to obtain in practice. Recent deep neural network (DNN)-based methods have been introduced to address this; yet they often suffer from high inference complexity. This paper proposes an Attention-aided MMSE (A-MMSE), a model-based DNN framework that learns the linear MMSE filter via the Attention Transformer. Once trained, the A-MMSE performs channel estimation through a single linear operation, eliminating nonlinear activations during inference and thus reducing computational complexity. To improve the learning efficiency of the A-MMSE, we develop a two-stage Attention encoder that captures the frequency and temporal correlation structure of OFDM channels. We also introduce a rank-adaptive extension that enables a flexible performance-complexity trade-off. Numerical simulations show that the proposed A-MMSE consistently outperforms other baseline methods in terms of normalized MSE across a wide range of signal-to-noise ratio (SNR) conditions. In particular, the A-MMSE and its rank-adaptive extension provide an improved performance-complexity trade-off, providing a powerful and highly efficient solution for practical channel estimation.

Index Terms—Orthogonal frequency division multiplexing (OFDM), Channel estimation, Minimum mean-squared error (MMSE), Attention Transformer, Deep learning

I. INTRODUCTION

Orthogonal frequency division multiplexing (OFDM) is a foundational waveform in modern wireless communication systems. OFDM was initially adopted in earlier standards such as Wi-Fi (IEEE 802.11), WiMAX, and was later introduced into the 3GPP-based cellular ecosystem with LTE. This adoption paved the way for OFDM’s continued prominence in 5G [1], [2] and its expected role in future 6G technologies [3].

One of the critical problems in OFDM is channel estimation, which is essential for enabling coherent detection. The goal of OFDM channel estimation is to accurately estimate the channel state information for each subcarrier using noisy

pilot symbols. A classical solution for the OFDM channel estimation involves signal processing (SP)-based approaches, including least squares (LS) and linear minimum mean-squared error (LMMSE) estimation methods [4], [5]. LS is simple to implement, but its performance is limited because it cannot incorporate prior OFDM channel statistics. LMMSE, in contrast, requires second-order statistics, such as noise variance and correlation across subcarriers, which are difficult to obtain accurately in practical scenarios [6].

Recently, inspired by the remarkable success of deep neural networks (DNNs) across various engineering fields, DNN-aided channel estimation for OFDM has gained considerable attention. DNNs, as pre-trained neural network models, can effectively capture complex data relationships without explicit prior statistical knowledge. Leveraging this data-driven approach, several prior works have explored DNN-aided OFDM channel estimation strategies. In [7], an OFDM channel slot was treated as image data. Based on this, a super-resolution network and a denoising neural network were simultaneously employed to estimate the OFDM channel (i.e., ChannelNet). In [8], using a similar modeling approach to [7], ReEsNet [8] was proposed, where a residual learning-based DNN was used to reconstruct the OFDM channel. This method achieves lower computational cost and higher accuracy than [7]. In [9], a residual convolutional network combined with bilinear interpolation was proposed for OFDM channel estimation, offering enhanced flexibility to varying pilot patterns and reduced complexity. Beyond deterministic models, [10] optimized a deep generative model using compressive pilot measurements for high-dimensional channel estimation. This method leverages learned priors to reduce pilot overhead and surpass traditional sparse recovery techniques.

In particular, with the advent of the Attention Transformer architecture [11], some recent works investigated Transformer models as a compelling solution for wireless channel estimation problems, owing to their representational capacity. In [12], super-resolution techniques were integrated with an Attention-based encoder-decoder framework to enhance OFDM channel estimation accuracy. In [13], Channelformer was developed, where an Attention-based encoder-decoder neural architecture was designed to incorporate input precoding. A common structure in prior studies using DNNs for channel estimation [7]–[10], [12], [13] is the use of a pre-trained neural network that directly maps noisy pilot signals to the estimated channel matrix, as illustrated in the left panel of Fig. 1.

Despite their significant advantages over classical SP-based channel estimation methods, existing DNN-based approaches have several limitations. We summarize these as follows.

This work was supported in part by the 6GARROW project funded by the Smart Networks and Services Joint Undertaking (SNS JU) under the European Union’s Horizon Europe research and innovation programme (Grant Agreement No. 101192194) and by an IITP grant funded by the Korean government (MSIT) (No. RS-2024-00435652); in part by an IITP grant funded by MSIT (No. RS-2024-00395824, “Development of Cloud-virtualized RAN (vRAN) system supporting upper-midband”); and in part by the IITP Digital Innovation Talent Short-Term Intensive Program grant funded by MSIT (No. RS-2024-00404972).

The authors are with School of Electrical and Electronic Engineering, Yonsei University, South Korea (e-mail: t.jha@yonsei.ac.kr, jch0624@yonsei.ac.kr, garksill@yonsei.ac.kr, simyffff@yonsei.ac.kr, jhpark@yonsei.ac.kr)

- **Computational overhead:** Typically, DNN-based models involve a large number of parameters (approximately 53,000 for ReEsNet [8] and 110,000 for Channelformer [13]), leading to significant computational and memory overhead per channel estimation. Furthermore, several nonlinear operations are used (e.g., ReLU [14], tanh [15], ELU [16], and pooling [17]), limiting hardware acceleration effectiveness. These nonlinearities, although essential for model expressiveness, may introduce additional computational overhead and pose challenges related to inference complexity and practical implementation.
- **Limited interpretability:** Existing DNN-based approaches are typically applied directly to OFDM channel estimation in a purely data-driven manner, without incorporating domain knowledge derived from mathematical models. However, studies such as [18], [19] showed that integrating domain-specific insights into neural network design can lead to notable performance gains over purely data-driven methods. This implies that considerable potential remains to further push performance boundaries by leveraging domain-specific insights.
- **Lack of flexibility:** For practical deployment, it is often desirable for channel estimation methods to adaptively adjust computational load. For example, assuming a scenario where a user has severely constrained processing resources, the estimator should be able to reduce its complexity by adjusting the number of parameters. However, most existing DNN-based approaches lack this adaptability, as they provide no explicit mechanisms to control the model size or computational cost within the DNN architecture.

We note that these limitations primarily arise from employing DNNs as end-to-end channel estimators, where the model learns a direct mapping from noisy pilot signals to channel estimates solely based on data.

To address the challenges of purely data-driven approaches, recent research has actively explored the concept of model-based DNNs [20]. The core idea is to leverage a hybrid method that combines classical SP-based approaches and data-driven DNN-based approaches, thereby harnessing the advantages of both methodologies, i.e., powerful learning capability and mathematical interpretability. For instance, [21] proposed KalmanNet, where the Kalman gain matrix is learned using recurrent neural network architectures such as long short-term memory (LSTM) [22] or gated recurrent units (GRU) [23], while retaining the recursive update structure of the classical Kalman filtering algorithm [24]. Thanks to its hybrid design, KalmanNet [21] effectively addresses the state estimation problem, even with partially known state models. Subsequently, several extensions were proposed, including [25]–[28]. In parallel, model-based DNN approaches have been widely applied to various tasks, such as multiple-input multiple-output (MIMO) beamforming design [29], and MIMO detection [19], [30]. However, to the best of our knowledge, no model-based DNN framework has been explored for OFDM channel estimation. This work addresses this notable gap by devising a novel channel estimation method

that leverages not only the learning capability of DNNs, but also domain knowledge from classical SP-based approaches.

In this paper, we propose an Attention-aided MMSE (A-MMSE) method for OFDM channel estimation. The key idea is to exploit the Attention Transformer architecture to learn linear channel estimation filter coefficients, rather than directly estimating the OFDM channel outputs using DNNs. The fundamental difference between conventional DNN-based approaches and the proposed method is illustrated in Fig. 1. Once the linear filters are trained using the Attention Transformer, the proposed A-MMSE performs channel estimation solely by relying on a linear process, effectively decoupling the estimation mechanism from the learning procedure. Building on the linear estimation structure of the A-MMSE, we further extend it by enabling rank-adaptive capability, referred to as the rank-adaptive A-MMSE (RA-A-MMSE). By adjusting the rank of the RA-A-MMSE estimation filter matrix, we achieve additional reductions in computational overhead with minimal loss in channel estimation accuracy.

In addition to the proposed A-MMSE structure, we also develop a novel two-stage Attention encoder to further enhance the channel estimation performance. Specifically, we first observe that the OFDM channel’s correlation matrix can be effectively decomposed into frequency and temporal domain correlations. Building on this insight, our two-stage Attention encoder consists of Frequency Encoder and Temporal Encoder, each designed to capture the corresponding correlation structure. In particular, the Frequency Encoder exploits a Multi-Head Self-Attention mechanism combined with a linear embedding, whose dimension matches the number of subcarriers. Subsequently, the Frequency Encoder’s output features are projected to the Temporal Encoder, which also leverages Multi-Head Self-Attention with an embedding dimension matching the total number of OFDM channel elements. By sequentially integrating the Frequency and Temporal Attention encoder blocks, our method effectively reflects complementary relationships across the frequency and temporal domains, extracting highly relevant latent features. These refined features are then decoded by a residual fully-connected network, precisely mapping them to the linear filter coefficients of the proposed A-MMSE method. Thanks to the two-stage Attention structure, OFDM channels’ inherent correlation characteristics are effectively incorporated in a form particularly suitable for A-MMSE filter design, significantly enhancing the overall estimation performance.

Via numerical simulations across diverse COST2100 [31] models, we show that the proposed A-MMSE and RA-A-MMSE significantly outperform traditional SP-based approaches (e.g., LS and LMMSE) and recent DNN-based approaches (e.g., ChannelNet [7] and Channelformer [13]) in terms of channel estimation accuracy. In particular, the A-MMSE achieves approximately 56% lower normalized MSE (NMSE) compared to conventional LMMSE. We attribute these performance gains to the Attention Transformer’s ability to effectively capture nonstationary channel statistics, even under challenging high-mobility and frequency-selective fading conditions. Compared to Channelformer, the A-MMSE achieves approximately 72% lower NMSE. We note that

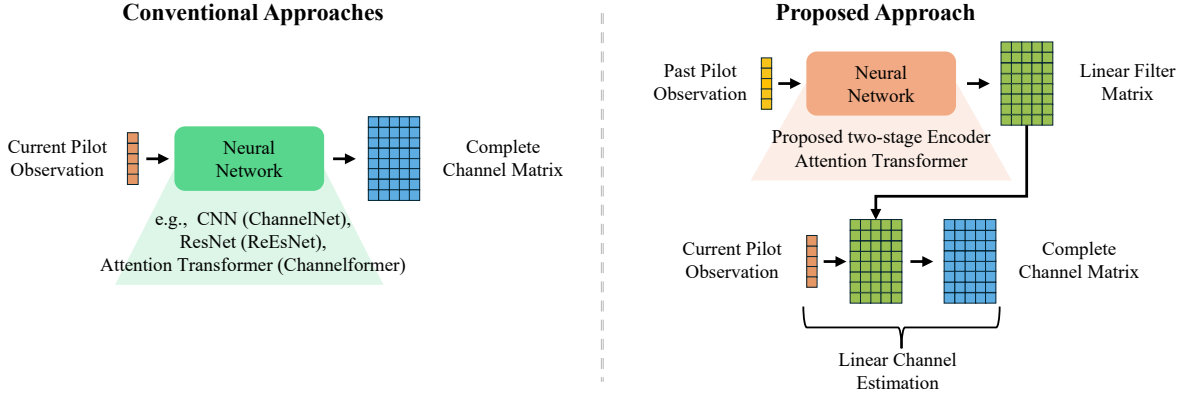


Fig. 1. Comparison of OFDM channel estimation structure: conventional approaches vs. the proposed A-MMSE approach.

these gains stem from our novel two-stage Attention encoder architecture, where frequency-domain features are first extracted and subsequently refined through temporal correlation modeling. Moreover, the RA-A-MMSE further reduces computational complexity through adaptive rank reduction, maintaining over 74.6% of the performance achieved by the full-rank A-MMSE. As a result, the RA-A-MMSE requires only 1.5% of the computational complexity of Channelformer or LMMSE (i.e., a 98.5% reduction), while achieving approximately 51% lower NMSE. The proposed methods also exhibit strong robustness to signal-to-noise ratio (SNR) mismatch, retaining robust performance across a wide range of unseen SNR conditions. This underscores the practical efficiency and suitability of the proposed method for real-world 5G/6G implementations.

The distinct benefits of the proposed A-MMSE are summarized as follows. First, A-MMSE employs a two-stage Attention encoder that effectively captures the correlation structure of OFDM channels, thereby improving channel estimation accuracy and robustness and achieving approximately 61% and 67% lower NMSE compared to LMMSE and Channelformer, respectively. Second, once trained, A-MMSE performs OFDM channel estimation using purely linear computations, which significantly reduces computational complexity compared to conventional DNN-based methods that rely heavily on non-linear operations. Third, the RA-A-MMSE extension enables dynamic complexity scaling, reducing computational complexity by up to 99.8% for resource-constrained implementations, thereby facilitating efficient and flexible deployment in practical systems.

The rest of the paper is organized as follows. Section II describes the basic system model, and Section III introduces the conventional channel estimation methods including the SP-based approaches and the DNN-based approaches. In what follows, Section IV presents the main concept of the proposed A-MMSE method, and Section V further extends it to the RA-A-MMSE. Numerical results are provided in Section VI, and Section VII concludes the paper.

Notations: We denote transpose by $(\cdot)^T$, Hermitian transpose by $(\cdot)^H$, complex conjugate by $(\cdot)^*$, column-wise vectorization by $\text{vec}(\cdot)$, real and imaginary parts of a complex quantity by $\Re(\cdot)$ and $\Im(\cdot)$, the magnitude by $|\cdot|$, and the

Euclidean and Frobenius norms by $\|\cdot\|_2$ and $\|\cdot\|_F$, respectively. Element-wise (Hadamard) multiplication is denoted by \circ , the Kronecker product by \otimes , and statistical expectation is written as $\mathbb{E}[\cdot]$. The set difference is denoted by \setminus , horizontal (row-wise) stacking by $[\cdot, \cdot]$, and vertical (column-wise) stacking by $[\cdot; \cdot]$.

II. SYSTEM MODEL

In this section, we explain the system model used in this paper. We focus on a single OFDM slot with M OFDM symbols, each comprising N subcarriers, for a total of NM resource elements. The channel's frequency response corresponding to the n -th subcarrier and the m -th symbol is denoted as $H[n, m]$. Assuming that the cyclic-prefix (CP) is removed, the received signal model in the frequency-domain is given by

$$Y[n, m] = H[n, m]X[n, m] + Z[n, m], \quad (n, m) \in \mathcal{T}, \quad (1)$$

where $X[n, m]$ is the transmitted signal, $Z[n, m]$ is the additive Gaussian noise, and \mathcal{T} denotes the set of all resource elements. We denote by \mathcal{P} the set of indices corresponding to the pilot signals, where $|\mathcal{P}| = L$. This indicates that a total of L pilot symbols are used for channel estimation. Accordingly, $X[n, m]$ is known to the receiver for $(n, m) \in \mathcal{P}$. Let \mathcal{D} be the set of indices corresponding to the data signals, such that $\mathcal{P} \cup \mathcal{D} = \mathcal{T}$. For notational convenience, we define \mathbf{H} as the channel matrix whose (n, m) -th element is $H[n, m]$, and similarly for \mathbf{Y} , \mathbf{X} , and \mathbf{Z} . Accordingly, the signal model (1) is equivalently expressed as

$$\mathbf{Y} = \mathbf{H} \circ \mathbf{X} + \mathbf{Z}. \quad (2)$$

5G NR specifies the configuration of OFDM slots. For instance, in a standard OFDM resource block configuration with a normal cyclic prefix (CP) and subcarrier spacing of 30 kHz, each resource block comprises 12 subcarriers in frequency and 14 OFDM symbols in time. In this structure, with a typical Type-A demodulation reference signal (DM-RS) configuration for the physical downlink shared channel (PDSCH), the DM-RS can be inserted into two OFDM symbols, commonly at symbol indices 2 and 11, depending on the configured DM-RS pattern. All resource elements in other symbols are typically allocated for data. We generally follow 5G NR PDSCH configuration setup, but note that our

approach is also applicable to arbitrary configurations beyond this standard setting.

The OFDM channel estimation problem aims to estimate the channel matrix \mathbf{H} , denoted by $\hat{\mathbf{H}}$, given the observations \mathbf{Y} and the known pilot signal $X[n, m]$ at $(n, m) \in \mathcal{P}$. The NMSE is commonly adopted as the performance metric, defined as

$$\text{NMSE}(\hat{\mathbf{H}}) = \frac{\mathbb{E} [\|\mathbf{H} - \hat{\mathbf{H}}\|_F^2]}{\mathbb{E} [\|\mathbf{H}\|_F^2]}. \quad (3)$$

We note that the channel estimation process typically consists of denoising the observed pilot measurements, followed by interpolation or extrapolation to infer the channel coefficients at other resource elements in \mathcal{D} .

III. CONVENTIONAL CHANNEL ESTIMATION APPROACHES

In this section, we introduce conventional approaches to the OFDM channel estimation. Existing methods can be broadly categorized into two classes: SP-based approaches and DNN-based approaches.

A. SP-based Approach

SP-based OFDM channel estimation strategies have been extensively studied in [6]. Among the various approaches, this work intentionally focuses on pilot-assisted channel estimation, due to its robustness and practicality in wireless communication scenarios. In particular, the LS and MMSE estimators are commonly used as standard methods.

LS: The LS method aims to directly minimize the errors between the received signal and the transmitted pilot signals. Specifically, it seeks to find

$$\hat{\mathbf{H}}_{\text{LS}} = \arg \min_{H[n, m], (n, m) \in \mathcal{P}} \sum_{(n, m) \in \mathcal{P}} |Y[n, m] - H[n, m]X[n, m]|^2, \quad (4)$$

which leads to the following closed-form solution at the pilot positions:

$$\hat{H}[n, m] = \frac{Y[n, m]}{X[n, m]}, \quad (n, m) \in \mathcal{P}. \quad (5)$$

After obtaining the LS estimates at pilot positions, a subsequent interpolation (or extrapolation) step is typically applied to estimate the channel at non-pilot positions $(n, m) \in \mathcal{T} \setminus \mathcal{P}$. Various interpolation techniques can be employed, ranging from simple linear or bilinear interpolation [4], [32].

The LS estimator requires no prior statistical knowledge of the channel or noise, making it simple and straightforward to implement. However, its performance may degrade significantly, especially at low SNR conditions or when the channel matrix \mathbf{H} is ill-conditioned.

LMMSE: The LMMSE estimation uses prior channel statistics to minimize the expected MSE between the true channel and its estimate. It corresponds to the Bayesian conditional mean of the channel given the pilot observations, thus providing a statistically optimal solution to the channel estimation problem. This is given by

$$\hat{\mathbf{H}}_{\text{LMMSE}} = \arg \min_{\hat{\mathbf{H}}} \mathbb{E} [\|\mathbf{H} - \hat{\mathbf{H}}\|_F^2 | Y[n, m], (n, m) \in \mathcal{P}] \quad (6)$$

$$= \mathbb{E} [\mathbf{H} | Y[n, m], (n, m) \in \mathcal{P}], \quad (7)$$

where the expectation is taken over the randomness of \mathbf{H} and \mathbf{Z} . Assuming that \mathbf{H} and \mathbf{Z} are jointly Gaussian, the conditional mean (7) is given by the following linear expression:

$$\begin{aligned} \text{vec}(\hat{\mathbf{H}}_{\text{LMMSE}}) &= \mathbb{E} [\mathbf{H} | Y[n, m], (n, m) \in \mathcal{P}] \\ &= \mathbf{R}_{\text{vec}(\mathbf{H})\mathbf{H}_p} \mathbf{R}_{\mathbf{Y}_p\mathbf{Y}_p}^{-1} \mathbf{Y}_p, \end{aligned} \quad (8)$$

where $\text{vec}(\mathbf{H}) \in \mathbb{C}^{NM}$ denotes the vectorized full channel matrix, and $\mathbf{H}_p \in \mathbb{C}^L$ represents the vectorized frequency response at the pilot positions. $\mathbf{R}_{\text{vec}(\mathbf{H})\mathbf{H}_p} \in \mathbb{C}^{NM \times L}$ represents the cross-covariance matrix between $\text{vec}(\mathbf{H})$ and \mathbf{H}_p , while $\mathbf{R}_{\mathbf{Y}_p\mathbf{Y}_p} \in \mathbb{C}^{L \times L}$ represents the auto-covariance matrix of \mathbf{Y}_p . More concretely, when \mathbf{Z} is independent and identically distributed Gaussian with variance σ^2 , (8) is further derived as

$$\text{vec}(\hat{\mathbf{H}}_{\text{LMMSE}}) = \underbrace{\mathbf{R}_{\text{vec}(\mathbf{H})\mathbf{H}_p} (\mathbf{R}_{\mathbf{H}_p\mathbf{H}_p} + \sigma^2 \mathbf{I})^{-1}}_{\mathbf{W}_{\text{LMMSE}} \in \mathbb{C}^{NM \times L}} \mathbf{Y}_p, \quad (9)$$

where $\mathbf{W}_{\text{LMMSE}}$ indicates the LMMSE filter. Accordingly, the estimate corresponding to the specific resource element (n, m) is given by $\hat{H}[n, m] = \mathbf{R}_{H[n, m]\mathbf{H}_p} (\mathbf{R}_{\mathbf{H}_p\mathbf{H}_p} + \sigma^2 \mathbf{I})^{-1} \mathbf{Y}_p$. In this paper, the LMMSE refers to the linear LMMSE estimator obtained in (8).

Under the joint Gaussian assumption, the LMMSE estimator is well-established to achieve optimal MSE performance. Unlike the LS estimator, it exploits knowledge of the covariance matrices $\mathbf{R}_{\text{vec}(\mathbf{H})\mathbf{H}_p}$ and $\mathbf{R}_{\mathbf{H}_p\mathbf{H}_p}$, which enable effective denoising and interpolation by accounting for channel correlations across time and frequency.

Despite its optimality under the Gaussian assumption, the LMMSE estimator incurs high computational complexity because of the high dimensionality of the covariance matrix $\mathbf{R}_{\text{vec}(\mathbf{H})\mathbf{H}_p} \in \mathbb{C}^{NM \times L}$. To address this issue, a low-complexity approximation, termed the 1D frequency-domain LMMSE (1D-LMMSE) estimator, was proposed. In this method, the temporal-domain channel correlation is neglected, so that only the frequency-domain correlation is taken into account for channel estimation. The 1D-LMMSE estimator is given as

$$\hat{\mathbf{H}}_{\text{1D-LMMSE}} = \mathbf{R}_{\mathbf{H}[\mathcal{K}]\mathbf{H}[\mathcal{P}]} (\mathbf{R}_{\mathbf{H}[\mathcal{P}]\mathbf{H}[\mathcal{P}]} + \sigma^2 \mathbf{I})^{-1} \hat{\mathbf{H}}_{\text{LS}}, \quad (10)$$

where $\mathbf{H}[\mathcal{P}]$ denotes the frequency response at the pilot indices and $\mathbf{H}[\mathcal{K}] \in \mathbb{C}^N$ denotes the full frequency response of all the subcarriers including the pilot component corresponding to $\mathbf{H}[\mathcal{P}]$.

Remark 1. Despite their solid theoretical foundations, SP-based methods have several limitations. For instance, LMMSE relies on prior knowledge of channel statistics, such as noise variance and channel correlation, which may be difficult to obtain or inaccurate in practical scenarios. Furthermore, LMMSE estimation requires matrix inversion, incurring significant computational overhead per channel estimation. Also, the performance of these methods tends to degrade in highly dynamic or nonlinear channel environments, limiting their adaptability and robustness.

B. DNN-based Approach

To address the limitations of SP-based approaches, DNN-based approaches have been actively explored as a data-driven alternative. The key idea behind existing DNN-based methods is to leverage DNNs as a denoiser and also an interpolator for channel estimation. Specifically, by modeling the DNN input as the noisy received pilot signal (i.e., \mathbf{Y}_p) and the output as the corresponding channel estimate (i.e., $\hat{\mathbf{H}}$), we train the DNN to learn a nonlinear mapping between \mathbf{Y}_p and $\hat{\mathbf{H}}$. Existing research on DNN-based approaches can be categorized according to the specific neural network architectures employed for channel estimation.

ChannelNet: The ChannelNet [7] represents one of the initial frameworks that exploits a DNN for OFDM channel estimation. In this approach, the channel response is treated as an image. An initial estimate of the channel is obtained by applying bilinear interpolation to sparsely located pilot symbols, resulting in a low-resolution and noise-contaminated channel map. Then, ChannelNet uses a super-resolution convolutional neural network (i.e., SRCNN) to recover high-resolution spatial features from the interpolated input. After this, a denoising convolutional neural network (i.e., DnCNN) is applied, incorporating residual learning and batch normalization to further refine the estimate.

Channelformer: The Channelformer [13] exploits the Attention Transformer architecture for OFDM channel estimation. Unlike ChannelNet, Channelformer flattens the LS channel estimate for all pilot subcarriers into a single vector and feeds its real and imaginary parts as two separate input channels. Based on this, the encoder captures long-range dependencies among sparse pilot embeddings using the Attention Transformer architecture. Instead of the standard Feed-Forward Network, it employs convolutional layers to introduce local inductive bias, while retaining global modeling capabilities through multi-head self-Attention. The decoder refines these context-aware features using a residual convolutional network, integrating both global Attention and local structural information.

To clarify the mechanism, we explain the principle of Channelformer as follows. Fundamentally, Channelformer follows the Multi-Head Self-Attention (MHA) mechanism [11]. To be specific, denoting p_i as the complex-valued channel observation at pilot index i with $1 \leq i \leq L$, each pilot observation is first embedded into a two-dimensional real-valued row vector that retains its inherent complex structure: $\mathbf{e}_i = [\Re(p_i), \Im(p_i)] \in \mathbb{R}^2$. Then, we define the full sequence of embedded pilot vectors as

$$\mathbf{X} = [\mathbf{e}_1^T, \dots, \mathbf{e}_L^T]^T \in \mathbb{R}^{L \times 2}, \quad (11)$$

where each row \mathbf{e}_i corresponds to a distinct pilot symbol. This representation serves as the input to the encoder module.

Then, the encoder begins by applying the MHA mechanism to capture local and global dependencies across the sparse pilot positions. Specifically, MHA is computed as:

$$\text{head}_i = \text{Attention}(\mathbf{Q}^{(i)}, \mathbf{K}^{(i)}, \mathbf{V}^{(i)}), \quad i = 1, \dots, h, \quad (12)$$

$$\mathbf{Z} = \text{Concat}(\text{head}_1, \dots, \text{head}_h) \mathbf{W}_O, \quad (13)$$

where $h = 2$, representing the number of symbols containing pilots and the Attention operation within each head is the Scaled Dot-Product Attention defined as

$$\text{Attention}(\mathbf{Q}^{(i)}, \mathbf{K}^{(i)}, \mathbf{V}^{(i)}) = \text{softmax} \left(\frac{\mathbf{Q}^{(i)} \mathbf{K}^{(i)T}}{\sqrt{d_k}} \right) \mathbf{V}^{(i)}. \quad (14)$$

In this formulation, d_k denotes the number of pilot elements within a symbol and each of the query ($\mathbf{Q}^{(i)}$), key ($\mathbf{K}^{(i)}$), and value ($\mathbf{V}^{(i)}$) matrices is obtained by applying linear projections of the input feature vectors as follows:

$$\mathbf{Q}^{(i)} = \mathbf{Z}_{\text{in}} \mathbf{W}_Q^{(i)}, \quad \mathbf{K}^{(i)} = \mathbf{Z}_{\text{in}} \mathbf{W}_K^{(i)}, \quad \mathbf{V}^{(i)} = \mathbf{Z}_{\text{in}} \mathbf{W}_V^{(i)}, \quad (15)$$

where \mathbf{Z}_{in} denotes the input feature matrix. $\mathbf{W}_Q^{(i)}, \mathbf{W}_K^{(i)}$, and $\mathbf{W}_V^{(i)}$ are learnable weight matrices corresponding to the i^{th} head. Additionally, \mathbf{W}_O denotes a weight matrix used for merging information across all heads.

Unlike the conventional Attention Transformer encoder that employs a position-wise Feed-Forward Network (FFN) following MHA, Channelformer introduces a convolutional layer to enhance local spatial modeling:

$$\mathbf{Z}' = \text{Conv}(\mathbf{Z}), \quad \mathbf{H}_{\text{enc}} = \text{Norm}(\mathbf{Z} + \mathbf{Z}'), \quad (16)$$

where \mathbf{H}_{enc} represents the final encoder output, enriched with both global and local contextual information. The rationale behind incorporating convolutional layers is to inject local inductive biases into the global Attention-based features, enabling the network to capture intricate local channel variations effectively.

The decoder maps the encoded representations to the full channel estimate through a residual convolutional neural network ($\mathcal{F}_{\text{ResCNN}}(\cdot)$):

$$\hat{\mathbf{H}} = \mathcal{F}_{\text{ResCNN}}(\mathbf{H}_{\text{enc}} | \theta_{\text{dec}}), \quad \hat{\mathbf{H}} \in \mathbb{C}^{N \times M}, \quad (17)$$

where θ_{dec} denotes the learnable parameters of the decoder.

Remark 2. DNN-based channel estimation approaches have several benefits. Notably, they do not require direct prior knowledge of channel statistics, which enhances their practical applicability. Additionally, the powerful learning capabilities of DNNs are able to capture the channel's correlation structures directly from training data, facilitating accurate channel estimation even in challenging scenarios such as high-mobility environments. Nonetheless, these approaches are limited by: i) a large number of model parameters and nonlinear computations, and ii) a lack of flexibility in easily adjusting the computational overhead according to the user's computation capability. We note that these shortcomings mainly arise because existing DNN-based architectures (including SRCNN and Attention Transformer) are directly used to produce channel estimation outputs. As a result, several nonlinear activation functions are unavoidable, and the number of model parameters is difficult to control.

IV. ATTENTION-AIDED MMSE

In this section, we propose the A-MMSE method for OFDM channel estimation. Our key idea is to learn linear estimation

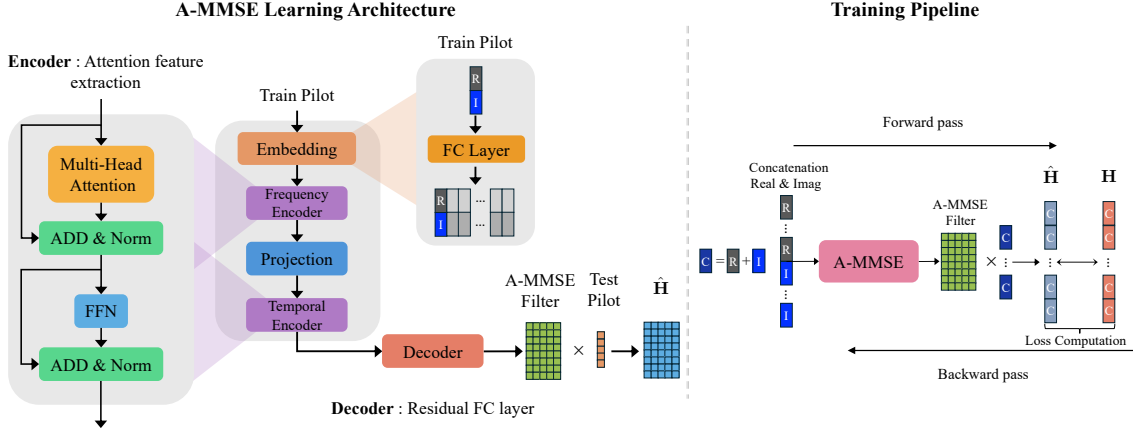


Fig. 2. Architecture and end-to-end training pipeline of the proposed A-MMSE network for learning the MMSE filter

filter coefficients using the Attention Transformer rather than directly employing a DNN to produce channel estimates. Once trained, the learned filters are applied to noisy pilot signals to yield channel estimates through a linear operation, resembling the structure of the classical SP-based MMSE estimation approach. In the following, we present a detailed explanation of the proposed A-MMSE method. For clarity of exposition, we first describe the A-MMSE estimation mechanism, followed by the A-MMSE learning mechanism.

A. A-MMSE Estimation Mechanism

In the proposed A-MMSE approach, channel estimation follows conventional linear processing. Specifically, the estimated channel matrix $\hat{\mathbf{H}}_{\text{A-MMSE}}$ is obtained by

$$\text{vec}(\hat{\mathbf{H}}_{\text{A-MMSE}}) = \mathbf{W}_{\text{A-MMSE}} \mathbf{Y}_p, \quad (18)$$

where $\mathbf{W}_{\text{A-MMSE}}$ represents the A-MMSE linear filter. The A-MMSE filter $\mathbf{W}_{\text{A-MMSE}}$ is learned through our Attention Transformer architecture as follows:

$$\mathbf{W}_{\text{A-MMSE}} = \mathcal{F}_{\text{A-MMSE}}([\mathfrak{R}(Y[n, m]); \mathfrak{I}(Y[n, m])], (n, m) \in \mathcal{P} | \theta_{\text{A-MMSE}}) \quad (19)$$

where $\mathcal{F}_{\text{A-MMSE}}(\cdot)$ represents the Attention Transformer network and $\theta_{\text{A-MMSE}}$ denotes learnable parameters of A-MMSE.

Remark 3. It is important to highlight several key points regarding the proposed A-MMSE method. First, by leveraging the Attention Transformer to learn $\mathbf{W}_{\text{A-MMSE}}$, A-MMSE inherits the primary advantages of DNN-based approaches: powerful learning capability and no requirement for prior channel statistics. Second, once $\mathbf{W}_{\text{A-MMSE}}$ is learned, we only use linear computation as presented in (18), avoiding the computational complexity associated with nonlinear activation functions in the channel estimation process. In this sense, the proposed A-MMSE is a hybrid approach that effectively combines SP-based and DNN-based approaches. Further, in the A-MMSE framework, it is possible to adjust the number of effective parameters within $\mathbf{W}_{\text{A-MMSE}}$, enabling the A-MMSE to adapt its computational overheads depending on various environments. We further explore this in the next section.

B. A-MMSE Learning Mechanism

1) *Insights on Two-Stage Attention Encoder:* We now provide a detailed explanation of the A-MMSE learning mechanism $\mathcal{F}_{\text{A-MMSE}}(\cdot)$ (19), whose overall architecture and training pipeline are depicted in Fig. 2. Structurally inspired by recent encoder-decoder architectures based on Attention Transformer, the proposed A-MMSE method incorporates theoretical insights derived from classical SP-based channel estimation approaches. Specifically, as shown in the MMSE filter structure (9), the optimal linear filter operates by first whitening the pilot observations and then interpolating the full OFDM channel using the underlying frequency-temporal-domain channel correlation. This highlights the importance of explicitly incorporating the channel's second-order statistics. The proposed A-MMSE learning mechanism effectively captures the correlation structure inherent to OFDM channels. Its detailed formulation is presented as follows.

Under the assumption of a wide-sense stationary uncorrelated scattering (WSSUS) environment and separable scattering function [33], the second-order statistics of OFDM channels exhibit a separable correlation function across frequency and temporal domains. Formally, the channel correlation matrix between two channel taps separated by frequency index difference Δn and time index difference Δm is factorized as follows:

$$\begin{aligned} \mathbf{R}_h(\Delta n, \Delta m) &= \mathbb{E}[\mathbf{H}[n, m]\mathbf{H}^*[n + \Delta n, m + \Delta m]] \\ &= r_f(\Delta n) \cdot r_t(\Delta m), \end{aligned} \quad (20)$$

where $r_f(\Delta n)$ and $r_t(\Delta m)$ represent the frequency-domain and temporal-domain correlation, respectively. Upon discretizing this correlation (20) over the OFDM grid, the covariance matrix of the OFDM channel is given by

$$\mathbf{R}_{\text{full}} = \mathbb{E}[\mathbf{h}\mathbf{h}^H] \approx \mathbf{R}_f \otimes \mathbf{R}_t \in \mathbb{C}^{NM \times NM}, \quad (21)$$

where \mathbf{h} denotes $\text{vec}(\mathbf{H}) \in \mathbb{C}^{NM}$, $\mathbf{R}_f \in \mathbb{C}^{N \times N}$ and $\mathbf{R}_t \in \mathbb{C}^{M \times M}$ represent the frequency and temporal domain correlation matrices, respectively, as visualized in Fig. 3. We note that the approximation (\approx) in (21) arises because the WSSUS assumption may not perfectly hold in practical scenarios. The representation of the full covariance matrix \mathbf{R}_{full} as the Kronecker product (\otimes) between the frequency-domain correlation

\mathbf{R}_f and the temporal-domain correlation \mathbf{R}_t (21) implies that the frequency- and temporal-domain correlation structure is separable. This allows for a compact and computationally efficient representation of the channel covariance matrix. Building on this insight, we propose the following two-stage encoder design.

- **Frequency Encoder:** In the Frequency Encoder stage, the pilot observations are processed along the subcarrier domain, extracting features on the frequency-domain correlation structure at pilot indices, corresponding to the rows of the matrix $\mathbf{R}_f[\mathcal{P}, :]$.
- **Temporal Encoder:** In the Temporal Encoder stage, the output of the Frequency Encoder is subsequently processed along the OFDM symbol domain, capturing temporal-domain correlation structures at pilot indices, corresponding to the rows of the matrix $\mathbf{R}_t[\mathcal{P}, :]$.

This two-stage encoder enables the model to learn the joint frequency–temporal correlation structure; each stage uses a single encoder block, which is critical for the accurate MMSE estimation. Crucially, we note that this encoder design represents a key distinction of the proposed A-MMSE learning mechanism compared to conventional DNN-based methods. Specifically, existing approaches typically adopt standard learning architectures such as CNNs [7] or Attention Transformers [13], without explicitly tailoring them to the statistical properties inherent in OFDM channels. In contrast, our method explicitly incorporates the inherent temporal and frequency-domain correlation structures of OFDM channels into the learning process. This integration not only enhances learning efficiency but also improves the model’s capability to generalize under practical channel conditions. In this sense, the proposed A-MMSE approach is distinguished not only by its design, which enables the learning of a linear estimation filter rather than directly estimating the OFDM channel matrix (as illustrated in Fig. 1), but also by its advanced learning mechanism that explicitly reflects the inherent correlation structure of OFDM channels.

2) *Multi-Head Self-Attention Mechanism:* Building upon the proposed two-stage encoder structure, we use the MHA mechanism in (12)–(15) to extract encoded features. In particular, the Frequency Encoder captures correlations between pilot observations and individual subcarriers, thus its number of attention heads is fixed to the pilot count within a single OFDM symbol. The Temporal Encoder then extends the resulting frequency-domain features along the symbol axis to model the inter-symbol correlation. Accordingly, the number of attention heads is set equal to the total number of OFDM symbols considered. The statistical features extracted by the two-stage encoder are subsequently passed through a residual fully connected decoder, which maps them into the coefficient space of the A-MMSE filter. The detailed process is as follows.

Frequency Encoder: The detailed structure of the two-stage encoder is depicted in Fig. 3. In the first stage, a linear embedding layer transforms the raw pilot input data into a high-dimensional embedding space, where the embedding dimension matches the number of subcarriers. This embedding is essential to facilitate the subsequent MHA mechanism, which effectively captures the frequency-domain dependencies

inherent among the pilot signals. Specifically, the noisy pilot vector is given by $\mathbf{x}_{\text{in}} = [x_1, x_2, \dots, x_{2L}]^T \in \mathbb{R}^{2L}$. Here, each scalar x_i is linearly embedded into a high-dimensional vector as: $\mathbf{x}_{\text{emb},i} = x_i \cdot \mathbf{P}_{\text{emb}} + \mathbf{b}_{\text{emb}}$, where $\mathbf{P}_{\text{emb}} \in \mathbb{R}^{1 \times d_e}$ is a learnable projection matrix and $\mathbf{b}_{\text{emb}} \in \mathbb{R}^{d_e}$ is a learnable bias vector. Stacking all $\mathbf{x}_{\text{emb},i}$, we have

$$\mathbf{X}_{\text{Emb}} = [\mathbf{x}_{\text{emb},1}^T, \mathbf{x}_{\text{emb},2}^T, \dots, \mathbf{x}_{\text{emb},2L}^T]^T \in \mathbb{R}^{2L \times d_e}. \quad (22)$$

The embedding dimension d_e is set equal to N (the number of subcarriers), ensuring that the resulting embedded representations effectively capture complex frequency-domain characteristics.

Subsequently, the embedding matrix \mathbf{X}_{Emb} is fed into the MHA module ($\mathcal{F}_{\text{MHA}}(\cdot)$) with the number of heads fixed at L , where L corresponds to the total number of DM-RS pilot symbols (one head per pilot). Each complete pilot is split into real and imaginary parts, resulting in the $2L$ column dimension of \mathbf{X}_{Emb} . For example, with Type-A DM-RS and additional Position = 1 (i.e., two DM-RS OFDM symbols) using a comb-2 pattern over 6 resource blocks (RBs), which has 72 subcarriers, there are $72/2 = 36$ pilots per DM-RS symbol, hence $L = 36 \times 2 = 72$ pilots in total. In general,

$$L = \left(\frac{N_{\text{RB}} \cdot N_{\text{SC/RB}}}{2} \right) \times N_{\text{DM-RS sym}}, \quad (23)$$

where N_{RB} is the number of resource blocks, $N_{\text{SC/RB}} = 12$ is the number of subcarriers per RB, and $N_{\text{DM-RS sym}}$ denotes the number of OFDM symbols carrying the DM-RS. The operation of the MHA module $\mathcal{F}_{\text{MHA}}(\cdot)$ is described in (12)–(15). We note that this allows each head to learn distinct frequency-domain correlation patterns. Following the MHA module, Add & Layer Normalization is applied, followed by a FFN, and subsequently another Add & Layer Normalization, in sequential order. Details on Add & Norm and FFN are provided in [11]. After these processes, the encoder extracts frequency-domain statistical information, which can be formally represented as

$$\mathbf{Y}_{\text{Freq}} = \mathcal{E}_{\text{Frequency}}(\mathcal{F}_{\text{MHA}}(\mathbf{X}_{\text{Emb}} | \theta_{\text{MHA, Freq}}) | \theta_{\text{Freq}}) \quad (24)$$

where $\mathbf{Y}_{\text{Freq}} \in \mathbb{R}^{2L \times N}$ represents features encoded by the Frequency Encoder, $\mathcal{E}_{\text{Frequency}}$ represents the Frequency Encoder module, and $\theta_{\text{MHA, Freq}}$ and θ_{Freq} denote the learnable parameters of MHA module and the combined parameters of the two Add & Layer Normalization and FFN, respectively. Correspondingly, the overall operation $\mathbf{x}_{\text{in}} \mapsto \mathbf{Y}_{\text{Freq}}$ yields a real-valued matrix, where each row corresponds to a pilot position and columns align with subcarrier-specific embedding dimensions, explicitly capturing both local and global dependencies in the frequency-domain.

Temporal Encoder: In the second stage, a linear projection layer transforms the features encoded in the previous stage into a high-dimensional frequency and temporal domain, where the projection dimension is NM . The encoded feature matrix is given as $\mathbf{Y}_{\text{Freq}} = [\mathbf{y}_{\text{freq},1}; \mathbf{y}_{\text{freq},2}; \dots; \mathbf{y}_{\text{freq},2L}] \in \mathbb{R}^{2L \times N}$. Here, each row vector $\mathbf{y}_{\text{freq},i}$ is linearly projected as $\mathbf{x}_{\text{proj},i} = \mathbf{y}_{\text{freq},i} \cdot \mathbf{P}_{\text{proj}} + \mathbf{b}_{\text{proj}}$, where $\mathbf{P}_{\text{proj}} \in \mathbb{R}^{N \times d_p}$ is a learnable projection

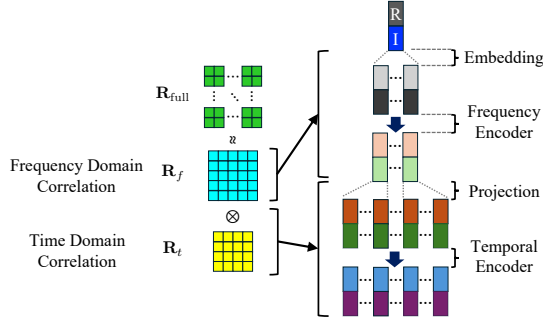


Fig. 3. Detailed structure of the proposed two-stage Attention encoder.

matrix and $\mathbf{b}_{\text{proj}} \in \mathbb{R}^{d_p}$ is a learnable bias vector. Stacking all projected vectors $\mathbf{x}_{\text{proj},i}$, this yields the matrix given by

$$\mathbf{X}_{\text{Proj}} = [\mathbf{x}_{\text{proj},1}^T, \mathbf{x}_{\text{proj},2}^T, \dots, \mathbf{x}_{\text{proj},2L}^T]^T \in \mathbb{R}^{2L \times d_p}. \quad (25)$$

We note that the projection dimension d_p is set to NM , ensuring that the model captures the frequency-temporal correlation of the OFDM channel, as formulated in (21).

Next, the projected matrix \mathbf{X}_{Proj} is fed into another MHA module, with the number of heads fixed at M (one head for each OFDM symbol). Similar to the above, this enables each head to effectively learn distinct temporal correlation patterns. The subsequent process is identical to that of the Frequency Encoder.

After completing all the steps, the frequency-temporal statistical information extracted by the Temporal Encoder can be represented as follows:

$$\mathbf{Y}_{\text{Temp}} = \mathcal{E}_{\text{Temporal}}(\mathcal{F}_{\text{MHA}}(\mathbf{X}_{\text{Proj}}|\theta_{\text{MHA, Temp}})|\theta_{\text{Temp}}) \quad (26)$$

where $\mathbf{Y}_{\text{Temp}} \in \mathbb{R}^{2L \times NM}$ represents features encoded by the Temporal Encoder, $\mathcal{E}_{\text{Temporal}}$ represents the Temporal Encoder module, with $\theta_{\text{MHA, Temp}}$ and θ_{Temp} being the learnable parameters of MHA module and the combined parameters of the two Add & Layer Normalization and FFN, respectively. The overall operations $\mathbf{Y}_{\text{Freq}} \mapsto \mathbf{Y}_{\text{Temp}}$ yield a real-valued matrix, whose rows correspond to pilot positions and whose columns align with subcarrier-symbol specific embedding dimensions. This explicitly captures both local and global dependencies in the frequency and temporal domain of the OFDM channel. The frequency-temporal features encoded by the two-stage encoder serve as inputs to the decoder.

Residual Fully Connected Decoder: Now we describe the decoder structure. The decoder of the A-MMSE model employs a residual fully connected (ResFC) module. Through this, we aim to reconstruct the final A-MMSE filter, from the encoded frequency-temporal features.

The decoder input, i.e., \mathbf{Y}_{Temp} , is processed through multiple fully connected layers with residual connections to ensure stable training and efficient transformation. The output dimension of the decoder remains consistent with its input dimension. This is presented as

$$\mathbf{Y}_{\text{Dec}} = \mathcal{F}_{\text{ResFC}}(\mathbf{Y}_{\text{Temp}}|\theta_{\text{ResFC}}) \in \mathbb{R}^{2L \times NM}, \quad (27)$$

where $\mathbf{Y}_{\text{Dec}} \in \mathbb{R}^{2L \times NM}$ represents the A-MMSE filter coefficients mapped by the ResFC decoder, and θ_{ResFC} denotes the learnable decoder parameters.

Once \mathbf{Y}_{Dec} is obtained, it is partitioned into the real and imaginary components as follows.

$$\mathbf{W}_{\text{real}} = \mathbf{Y}_{\text{Dec}}[1:L, :] \in \mathbb{R}^{L \times NM}, \quad (28)$$

$$\mathbf{W}_{\text{imag}} = \mathbf{Y}_{\text{Dec}}[L+1:2L, :] \in \mathbb{R}^{L \times NM}. \quad (29)$$

Then, the final complex-valued filter matrix is reconstructed by combining these two components as

$$\mathbf{W}_{\text{out}} = \mathbf{W}_{\text{real}} + j \mathbf{W}_{\text{imag}}, \quad \mathbf{W}_{\text{A-MMSE}} = \mathbf{W}_{\text{out}}^T \in \mathbb{C}^{NM \times L}. \quad (30)$$

This completes the end-to-end A-MMSE learning pipeline.

3) *Training Method:* The proposed A-MMSE model is trained in an end-to-end fashion as shown in the training pipeline of Fig. 2. The model parameters are optimized by minimizing a certain loss function, which quantifies the discrepancy between the estimated and true channel responses across the entire dataset:

$$\text{Loss} = \frac{1}{N_{\mathcal{B}} \times \mathcal{B}} \sum_{j=1}^{N_{\mathcal{B}}} \sum_{i=1}^{\mathcal{B}} \mathcal{L}(\hat{\mathbf{H}}_{i,j}, \mathbf{H}_{i,j}), \quad (31)$$

where $N_{\mathcal{B}}$ denotes the number of mini-batches and \mathcal{B} denotes the mini-batch size. In addition, $\mathbf{H}_{i,j}$ and $\hat{\mathbf{H}}_{i,j}$ represent the corresponding true channel matrix and estimated channel matrix, respectively. For the loss function $\mathcal{L}(\cdot)$, MSE or Huber loss can be chosen. We discuss this further in the next subsection. The loss function (31) is minimized via backpropagation and the Adam optimizer [34].

After training, one final A-MMSE filter is produced from the entire training dataset. This A-MMSE filter remains fixed and is consistently applied to all test data without further modification.

C. Discussions

Now we provide further insights regarding the proposed A-MMSE method.

1) *MSE and Huber Loss:* Possible choices for the loss function $\mathcal{L}(\cdot)$ include MSE and Huber loss [35]. We explain these as follows.

- **MSE:** For simplicity, we omit the mini-batch index j from (31). For a mini-batch of size \mathcal{B} , the MSE is defined as

$$\text{MSE} = \frac{1}{\mathcal{B}} \sum_{i=1}^{\mathcal{B}} \|\hat{\mathbf{H}}_i - \mathbf{H}_i\|_F^2,$$

with its gradient derived as $\nabla_{\hat{\mathbf{H}}_i} \text{MSE} = 2(\hat{\mathbf{H}}_i - \mathbf{H}_i)$. The loss is convex and smooth, facilitating straightforward optimization. However, its quadratic growth makes the loss sensitive to outliers, as a single large residual can dominate the objective, undermining robustness.

- **Huber Loss:** With residual $a_i = \hat{\mathbf{H}}_i - \mathbf{H}_i$ and transition threshold $\delta > 0$, Huber loss is defined as

$$L_{\delta}(a_i) = \begin{cases} \frac{1}{2}a_i^2, & |a_i| \leq \delta, \\ \delta\left(|a_i| - \frac{1}{2}\delta\right), & |a_i| > \delta, \end{cases}$$

with its gradient

$$\nabla_{\hat{\mathbf{H}}_i} L_{\delta}(a_i) = \begin{cases} a_i, & |a_i| \leq \delta, \\ \delta \text{sgn}(a_i), & |a_i| > \delta. \end{cases}$$

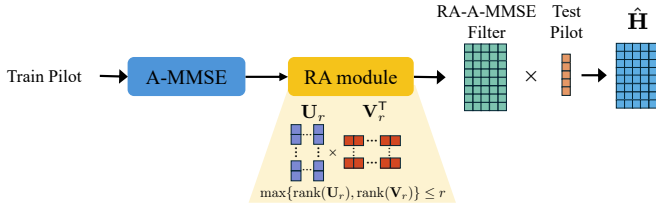


Fig. 4. RA-A-MMSE architecture: a rank-adaptation module is appended to A-MMSE to flexibly adjust the rank of the learned A-MMSE filter.

The loss function is quadratic near the origin and linear in the tails, limiting the influence of each outlier at $\mathcal{O}(\delta)$. In practice, δ can be chosen inversely proportional to the operating SNR, e.g., higher SNR implies cleaner observations and thus a smaller δ , whereas lower SNR favors a larger δ to mitigate noise-induced outliers.

To improve robustness to noise and extreme outliers, and better reflect channel statistics, we train A-MMSE with the Huber loss.

2) *Complexity*: The proposed A-MMSE is fundamentally distinguished from existing DNN-based channel estimation approaches. To be specific, the proposed A-MMSE method learns a linear filter matrix $\mathbf{W}_{\text{A-MMSE}}$ during a dedicated training phase. As a result, once trained, channel estimation reduces to a single matrix-vector multiplication, as shown in (18). This enables highly efficient inference, with minimal computational cost and requiring only $2(NM \times L)$ real-valued parameters to store $\mathbf{W}_{\text{A-MMSE}}$. In contrast, as discussed earlier, conventional DNN-based methods [7], [13] learn a neural network that maps pilot inputs directly to channel outputs. As a result, each inference (i.e., channel estimation) involves propagating the input through multiple layers of nonlinear operations, leading to higher inference complexity. Specifically, the A-MMSE performs channel estimation using only linear operations with approximately 70,000 ($= NM \times L$) parameters, whereas Channelformer requires about 110,000 parameters and includes nonlinear components, such as GELU activations and convolutional layers.

Nevertheless, the A-MMSE may still face challenges related to computational complexity and memory constraints especially as N, M or L increase. For example, despite its linear structure, storing the full matrix $\mathbf{W}_{\text{A-MMSE}}$ and performing large-scale matrix-vector multiplications can still be burdensome, particularly for users with limited computational resources. Hence, it is desirable to adapt the computation and memory requirements of A-MMSE depending on the available system resources. To this end, we propose a new technique that dynamically adjusts the filter structure, as detailed in the following section.

V. RANK-ADAPTIVE A-MMSE

In this section, by extending the A-MMSE, we introduce the RA-A-MMSE framework, whose architecture is illustrated in Fig. 4. The RA-A-MMSE incorporates a rank-adaptation mechanism that adaptively reduces the filter matrix rank according to resource constraints, such as a predefined maximum rank (r) or a limit on the number of filter parameters. By flexibly adjusting the rank to satisfy these constraints, the

RA-A-MMSE effectively reduces computational and memory overhead, allowing the filter to operate efficiently even under stringent computational resource limitations. Despite operating at a reduced rank, the RA-A-MMSE still maintains high estimation accuracy. It thus offers a practical and scalable solution for resource-constrained OFDM receivers, achieving a favorable balance between performance and hardware efficiency.

To explain the key idea of RA-A-MMSE, we begin by examining how rank reduction alleviates computational complexity. Recall that the A-MMSE filter $\mathbf{W}_{\text{A-MMSE}} \in \mathbb{C}^{NM \times L}$ is a linear transformation from the pilot observations to the channel estimate. Accordingly, without any rank-specific modification, the A-MMSE channel estimation requires linear operations proportional to $8NM \times L$, accounting for both real and imaginary components in complex-valued multiplications. Now suppose that the rank of $\mathbf{W}_{\text{RA-A-MMSE}}$ is reduced to r . Then the following rank- r factorization is allowed:

$$\mathbf{W}_{\text{RA-A-MMSE}} \approx \mathbf{A}\mathbf{B}^T, \quad \mathbf{A} \in \mathbb{C}^{NM \times r}, \quad \mathbf{B} \in \mathbb{C}^{L \times r}. \quad (32)$$

In this case, the estimation process can be decomposed into two sequential steps:

$$\tilde{\mathbf{Y}}_p = \mathbf{B}^T \mathbf{Y}_p, \quad \text{vec}(\hat{\mathbf{H}}_{\text{RA-A-MMSE}}) = \mathbf{A} \tilde{\mathbf{Y}}_p, \quad (33)$$

where $\mathbf{Y}_p \in \mathbb{C}^L$ is the pilot input and $\text{vec}(\hat{\mathbf{H}}_{\text{RA-A-MMSE}})$ is the channel estimate. This decomposition reduces the computational complexity to approximately $8rL + 8NM r$ real-valued operations, which is significantly lower than the full-rank case when $r \ll \min(NM, L)$.

To achieve the rank reduction in the RA-A-MMSE, we devise a rank-adaptive (RA) module that produces two trainable matrices, $\mathbf{U}_r \in \mathbb{R}^{NM \times r}$ and $\mathbf{V}_r \in \mathbb{R}^{L \times r}$, where r denotes the desired rank. With \mathbf{U}_r and \mathbf{V}_r , the A-MMSE filter matrix $\mathbf{W}_{\text{A-MMSE}}$ is modified to $\mathbf{W}_{\text{RA-A-MMSE}} = \mathbf{W}_{\text{A-MMSE}} \mathbf{U}_r \mathbf{V}_r^T$. Then the rank of $\mathbf{W}_{\text{RA-A-MMSE}}$ is bounded by

$$\text{rank}(\mathbf{W}_{\text{A-MMSE}} \mathbf{U}_r \mathbf{V}_r^T) \leq \min\{\text{rank}(\mathbf{W}_{\text{A-MMSE}}), \text{rank}(\mathbf{U}_r), \text{rank}(\mathbf{V}_r)\} \leq r, \quad (34)$$

where the last inequality holds if $r \leq \min\{NM, L\}$. As a result, the rank of $\mathbf{W}_{\text{RA-A-MMSE}}$ is bounded by r , allowing the effective filter rank to be adaptively controlled via the dimensions of \mathbf{U}_r and \mathbf{V}_r . This enables the RA-A-MMSE to flexibly adapt to available system resources. Compared to the A-MMSE, the computational cost reduction of the RA-A-MMSE can be quantified by the ratio:

$$\text{Complexity Cost Ratio: } \frac{\text{RA-A-MMSE}}{\text{A-MMSE}} \approx \frac{NM r + L r}{NML}. \quad (35)$$

Considering an OFDM channel comprising 6 RBs (minimum bandwidth assignment), i.e., $N = 72$, $M = 14$, the RA-A-MMSE with $r = 12$ reduces the computational cost by approximately 18% for $L = 72$. Moreover, since the RA module leverages learnable matrices (\mathbf{U}_r and \mathbf{V}_r) optimized during training, this substantial complexity reduction can be achieved with minimal channel estimation performance loss. We demonstrate this in the next section.

Remark 4. The proposed A-MMSE method exploits sparsity in two primary ways. First, the two-stage Attention encoder

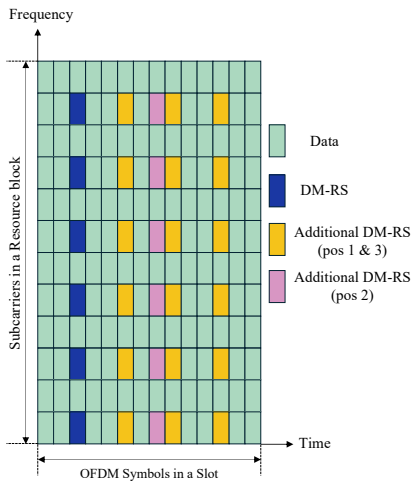


Fig. 5. 5G NR time-frequency resource block with Type A DM-RS.

implicitly leverages sparsity through its MHA mechanism, which naturally induces soft-sparsity by assigning higher weights to dominant features while suppressing less significant ones. This aligns well with wideband wireless channels that can be captured by a separable, low-rank covariance model ($\mathbf{R}_{\text{full}} \approx \mathbf{R}_f \otimes \mathbf{R}_t$). Second, the RA-A-MMSE framework exploits the rank-deficient structure inherent in the ideal LMMSE filter, where all rows share a common whitening filter and differ only by position-dependent correlation coefficients. By learning to identify and operate within this naturally sparse subspace, RA-A-MMSE achieves dramatic rank reduction without significant performance loss. As shown in Section VI, RA-A-MMSE preserves the majority of its performance under reduced-rank operation, demonstrating that it exploits the inherent low-dimensional structure of MMSE channel estimation rather than indiscriminately removing information.

VI. SIMULATION RESULTS

A. Simulation Setup

For numerical simulations, we adopt the 5G NR DM-RS configuration specified in 3GPP TS 38.211 [36]. As illustrated in Fig. 5, the DM-RS time-frequency density is adaptively configured to match channel dynamics, addressing the inherent trade-off between estimation accuracy and pilot overhead. We evaluate channel estimation performance using the geometry-based COST2100 model [31] in Semi-Urban (SU) and High-Speed Rail (HSR) scenarios (Table I). Note that we have also evaluated the proposed method using 3GPP-based TDL channel models. Owing to page limitations, these results are omitted from this paper but are available online [37].

For each scenario, 44,000 continuous OFDM frames were generated with dynamic Doppler updates. This continuous modeling creates a non-stationary environment where the global WSSUS assumption is explicitly broken, holding only

over short local intervals. To assess robustness against statistical drift, we employed a temporal split: the first 40,000 frames were allocated for training (36,000) and validation (4,000), while the subsequent 4,000 frames served as the test set. The model was implemented using TensorFlow on a single NVIDIA RTX 4090 GPU. We note that all the source code are available at [37]. The subcarrier spacings listed in Table I were specifically chosen to evaluate the trade-off between Doppler resolution and robustness to channel time-variations. For benchmarking, we compare our approach against SP-based estimators (LS, Oracle LMMSE, LMMSE mismatch, 1D-LMMSE, and sensing-aided estimation [38]) and DNN-based models (ChannelNet [7] and Channelformer [13]). In particular, the LMMSE mismatch computes the LMMSE filter based on an approximated channel covariance matrix learned from training samples, which results in a mismatch with the true channel statistics.

B. Normalized MSE Comparison

For the channel estimation performance comparison, we present the NMSE across different SNR levels in Fig. 6. The results derived from the COST2100 channel model encompass both the SU scenario shown in Fig. 6(a) and the HSR scenario shown in Fig. 6(b). As indicated by the results, the proposed framework achieves lower estimation errors compared to the conventional SP-based and DNN-based baselines across the evaluated channel conditions. Specifically, in the SU scenario, characterized by rich scattering and non-stationary statistics, the A-MMSE achieves an NMSE of 2.07×10^{-5} at an SNR of 35 dB. This corresponds to a reduction of approximately 73.8% compared to the mismatched LMMSE estimator (7.91×10^{-5}) and 82.2% compared to Channelformer (1.16×10^{-4}).

The significant performance gains of the proposed method over the mismatched LMMSE stem from the non-stationary nature of the considered channel environment. As described in Subsection VI-A, the WSSUS assumption does not hold globally, and channel statistics vary across OFDM frames. This directly causes covariance mismatch in conventional LMMSE estimation, as the filter relies on a fixed estimated covariance $\tilde{\mathbf{R}}$ while the true covariance \mathbf{R} changes over time. The conventional LMMSE estimator suffers from an unavoidable performance penalty due to this mismatch, quantified as

$$\Delta_{\text{mis}} = \left\| (\mathbf{W}_{\text{mis}} - \mathbf{W}^*) \Sigma_{\text{yy}}^{1/2} \right\|_F^2 \geq 0. \quad (36)$$

where \mathbf{W}_{mis} denotes the mismatched filter and \mathbf{W}^* represents the oracle LMMSE filter with perfect covariance knowledge. This penalty is proportional to $\|\Delta \mathbf{R}\|_F^2$ and establishes a fundamental performance floor, which is particularly severe in high-mobility environments such as the COST2100 HSR scenario. In contrast, A-MMSE bypasses the mismatch problem by learning the optimal filter directly from data, effectively capturing non-stationary channel correlations.

TABLE I
CONFIGURATION PARAMETERS FOR HSR AND SEMI-URBAN SCENARIOS

Scenario	Freq. (f_c)	Delay Spread	SCS	Velocity (v)	Max Doppler	Propagation
HSR	5 GHz	100 ns	60 kHz	350 km/h	≈ 1620.4 Hz	Strong LoS ($K = 13$ dB)
Semi-Urban	3.5 GHz	1000 ns	30 kHz	40 km/h	≈ 129.6 Hz	Rich Scattering ($K = 3$ dB)

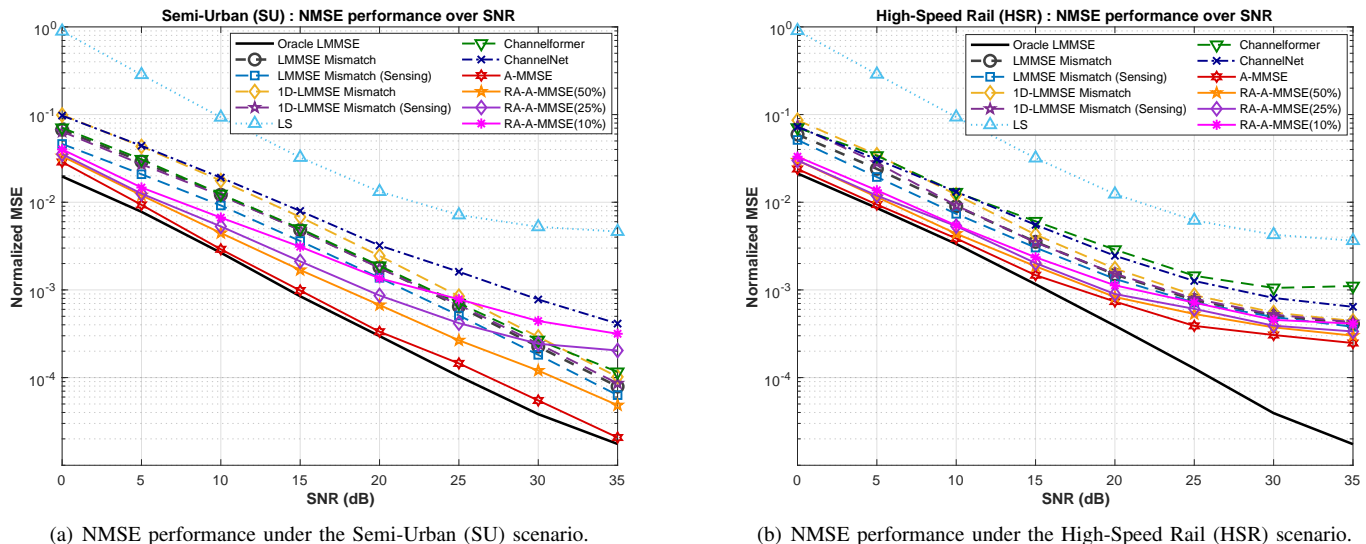


Fig. 6. NMSE performance comparison of various channel estimation methods over SNR under COST2100 channel models

Similar to the SU scenario, in the HSR scenario characterized by high-mobility (350 km/h), the A-MMSE yields an NMSE of 2.48×10^{-4} at 35 dB. This represents a reduction of approximately 39.4% compared to the mismatched LMMSE (4.09×10^{-4}).

Regarding the RA-A-MMSE, the results indicate that the model retains estimation performance comparable to the full-rank model, even with the reduced filter rank. In the HSR scenario, the RA-A-MMSE with 50% rank achieves an NMSE of 3.01×10^{-4} at 35 dB. This corresponds to approximately 82.4% of the estimation accuracy of the full-rank A-MMSE (2.48×10^{-4}), suggesting that the dominant low-rank structure arising from the strong line-of-sight (LoS) component is effectively captured despite the reduced parameters. Similarly, in the SU scenario, the RA-A-MMSE with 50% rank shows stable estimation accuracy, yielding an NMSE of 4.84×10^{-5} at 35 dB. Although the channel exhibits rich scattering, our method maintains an absolute NMSE in the order of 10^{-5} (same as original performance) while reducing computational complexity. These observations demonstrate the feasibility of the RA-A-MMSE to balance estimation fidelity and efficiency across different propagation environments.

Remark 5. We also compare our method against a sensing-aided approach [38], which serves as an advanced SP-based baseline. While this sensing-aided scheme effectively mitigates covariance mismatch—reducing NMSE by approximately 24% (SU) and 12% (HSR) compared to the standard mismatched LMMSE—the proposed A-MMSE significantly outperforms it. Specifically, the A-MMSE achieves an additional NMSE reduction of approximately 65% and 46% in SU and HSR scenarios, respectively, compared to the sensing-aided baseline. This confirms that the data-driven filter learning of A-MMSE offers superior adaptability over purely SP-based refinements.

C. Robustness to SNR Mismatch

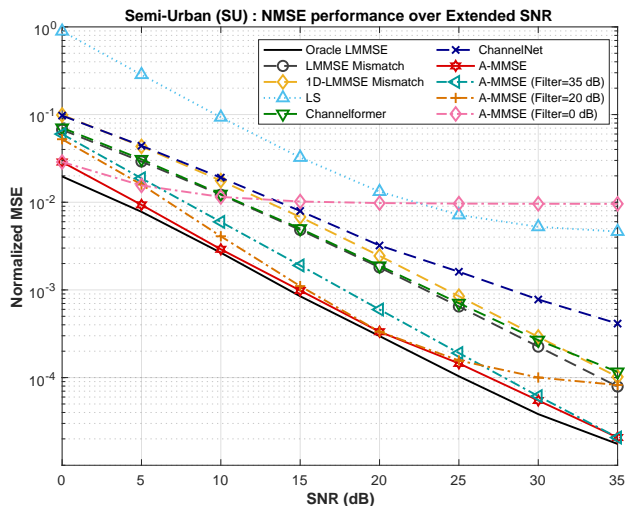
To evaluate the robustness of A-MMSE under SNR mismatch, we examine the performance of models trained at fixed SNRs of 0 dB, 20 dB, and 35 dB across the full SNR range (Fig. 7). We observe that models trained at extreme SNRs fail to generalize effectively. Specifically, the model trained at 0 dB hits an early error floor in the high-SNR regime, yielding an NMSE of 9.6×10^{-3} in the SU scenario (Fig. 7(a)) at 35 dB—approximately 460 times worse than the matched baseline—because the network prioritizes noise suppression over feature extraction. Conversely, the 35 dB model suffers in low-SNR conditions due to a lack of noise regularization, exhibiting a 6.7-fold NMSE degradation in the HSR scenario (Fig. 7(b)) at 0 dB (0.16 versus 0.024).

In contrast, the model trained at 20 dB achieves a robust trade-off, effectively providing a good operating point. It maintains consistent performance across the entire dynamic range, with only marginal degradation at 35 dB (e.g., maintaining NMSE within a factor of 1.5 of the matched baseline in the HSR scenario). We attribute this to the fact that moderate noise serves as regularization, allowing the network to strike a favorable balance between denoising capability and performance in low noise regimes.

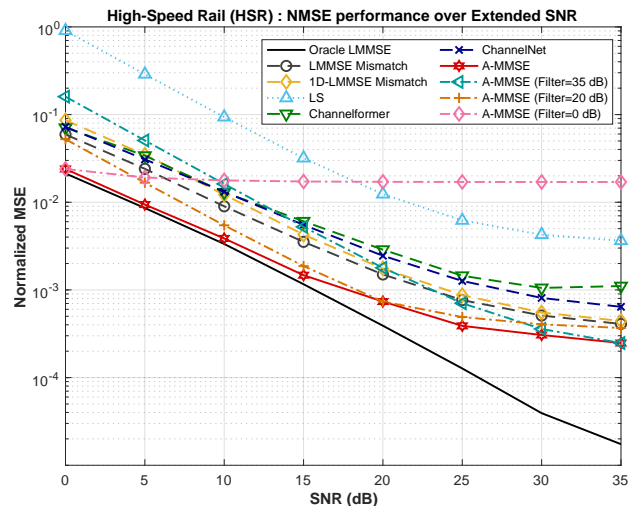
We have additionally conducted robustness evaluations under channel-scenario mismatch and developed an online A-MMSE framework to adapt to such conditions. Due to page limitations, these results are provided only online [37].

D. Performance-Complexity Trade-off

In this subsection, we evaluate computational complexity of each channel estimation method in terms of floating-point operations (FLOPs). FLOPs quantify the number of arithmetic operations required for inference (i.e., channel estimation). For example, one complex multiplication consists of four real multiplications and two real additions, totaling six real FLOPs. We note that training complexity is not considered in this analysis, as it is performed offline and has little impact on the real-time inference costs during deployment.



(a) NMSE performance under the Semi-Urban Scenario over full SNR



(b) NMSE performance under the High-Speed Rail Scenario over full SNR

Fig. 7. NMSE performance comparison of various channel estimation methods over extended SNR under COST2100 channel models

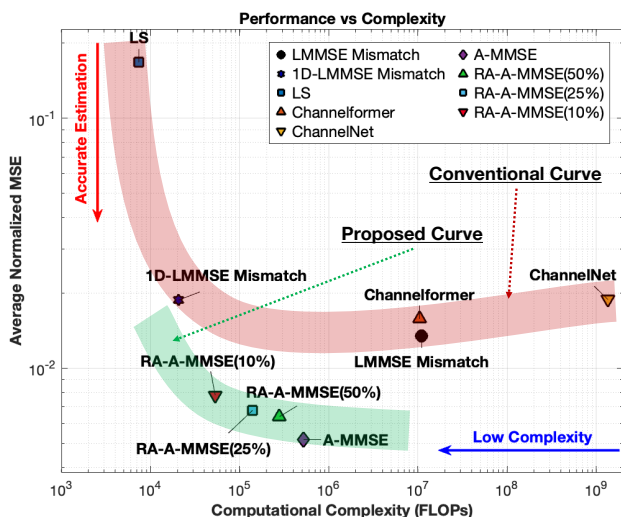


Fig. 8. NMSE–complexity trade-off across channels for the proposed and conventional estimators

Fig. 8 illustrates the trade-off between the average NMSE and computational complexity, averaged across all SNR levels and both HSR and SU scenarios. We also summarize the performance FLOPs for all the considered methods in Table II. As shown in Fig. 8, the proposed A-MMSE achieves superior channel estimation performance with substantially lower computational complexity. Specifically, it yields around 64.5% lower average NMSE and 95.1% fewer FLOPs compared to the average performance of LMMSE and Channelformer.

The rank-adaptive extension further optimizes this efficiency. The RA-A-MMSE with 10% rank retains high accuracy despite the reduced rank, achieving approximately 50.5% lower average NMSE compared to Channelformer. This demonstrates that the RA-A-MMSE effectively exploits the estimator’s low-rank structure, offering a scalable solution that outperforms DNN baselines with reduced computational overhead. As discussed, these benefits arise from the fact that A-MMSE relies solely on computationally efficient linear

TABLE II
FLOPS COMPARISON FOR CHANNEL ESTIMATION ($L = 72$)

Method	Computational Cost (FLOPs)
LMMSE	≈ 21 M
1D-LMMSE	≈ 41 K
LS	≈ 15 K
ChannelNet	≈ 1.35 G
Channelformer	≈ 21 M
A-MMSE	≈ 5.8 K
RA-A-MMSE	$\approx 8608r$, $r = \text{rank}$

operations during channel estimation. Consequently, the A-MMSE and RA-A-MMSE frameworks advance the performance–complexity trade-off, achieving improved estimation accuracy at significantly reduced computational cost. This establishes a practical benchmark for channel estimation by enhancing the trade-off between accuracy and efficiency.

VII. CONCLUSION

In this paper, we proposed the A-MMSE method for OFDM channel estimation. Our key idea is to integrate the classical SP-based framework with the learning capability of the DNN-based approach. Specifically, the proposed A-MMSE learns the linear filtering matrix via the Attention Transformer and applies it for channel estimation, achieving both high estimation accuracy and substantial computational efficiency. In particular, to enhance the learning of the linear filtering matrix, we developed a novel two-stage Attention encoder that effectively captures the frequency and temporal correlation structures of the OFDM channel. Building on this architecture, we further introduced a rank-adaptive extension of A-MMSE, referred to as the RA-A-MMSE. The RA-A-MMSE is distinguished by dynamically adjusting the rank of the linear filtering matrix, thereby controlling the computational overhead associated with channel estimation. Through extensive numerical simulations using COST2100 channel models, we demonstrated that the proposed A-MMSE provides significant performance gains in channel estimation

compared to conventional SP-based methods as well as DNN-based methods. We further showed that the RA-A-MMSE effectively balances estimation performance and computational complexity, offering substantial reductions in computational overhead with minimal performance degradation.

The proposed A-MMSE and the RA-A-MMSE frameworks offer several key advantages: i) once trained, only the linear filter is used, resulting in architectural simplicity; ii) by leveraging the representation learning capability of the Attention Transformer, they effectively capture the intrinsic correlation structure of wireless channels; and iii) they provide a principled integration of classical signal processing with deep learning. With its efficient design, the A-MMSE aligns well with emerging 6G physical-layer principles, emphasizing scalability and AI-native architectures.

Future work may extend this framework to scenarios where ground-truth channel information is unavailable during training. In addition, exploring reinforcement learning paradigms that leverage end-to-end performance metrics, such as log-likelihood ratios (LLRs), represents a promising direction. Extending our framework to MIMO-OFDM channel acquisition [39] is also interesting.

REFERENCES

- [1] M. Shafi, A. F. Molisch, P. J. Smith, T. Haustein, P. Zhu, P. De Silva, F. Tufvesson, A. Benjebbour, and G. Wunder, "5G: A tutorial overview of standards, trials, challenges, deployment, and practice," *IEEE J. Sel. Areas Commun.*, vol. 35, no. 6, pp. 1201–1221, 2017.
- [2] P. Guan, D. Wu, T. Tian, J. Zhou, X. Zhang, L. Gu, A. Benjebbour, M. Iwabuchi, and Y. Kishiyama, "5G field trials: OFDM-based waveforms and mixed numerologies," *IEEE J. Sel. Areas Commun.*, vol. 35, no. 6, pp. 1234–1243, 2017.
- [3] S. D. Liyanaarachchi, T. Riihonen, C. B. Barneto, and M. Valkama, "Optimized waveforms for 5G–6G communication with sensing: Theory, simulations and experiments," *IEEE Trans. Wireless Commun.*, vol. 20, no. 12, pp. 8301–8315, 2021.
- [4] O. Edfors, M. Sandell, J.-J. van de Beek, S. Wilson, and P. Borjesson, "OFDM channel estimation by singular value decomposition," *IEEE Trans. Commun.*, vol. 46, no. 7, pp. 931–939, 1998.
- [5] Y. Li, "Pilot-symbol-aided channel estimation for OFDM in wireless systems," *IEEE Trans. Veh. Technol.*, vol. 49, no. 4, pp. 1207–1215, 2000.
- [6] Y. Liu, Z. Tan, H. Hu, L. J. Cimini, and G. Y. Li, "Channel estimation for OFDM," *IEEE Commun. Surveys & Tutorials*, vol. 16, no. 4, pp. 1891–1908, 2014.
- [7] M. Soltani, V. Pourahmadi, A. Mirzaei, and H. Sheikhzadeh, "Deep learning-based channel estimation," *IEEE Commun. Lett.*, vol. 23, no. 4, pp. 652–655, 2019.
- [8] L. Li, H. Chen, H.-H. Chang, and L. Liu, "Deep residual learning meets OFDM channel estimation," *IEEE Wireless Commun. Lett.*, vol. 9, no. 5, pp. 615–618, 2020.
- [9] D. Luan and J. Thompson, "Low complexity channel estimation with neural network solutions," in *Proc. 25th International ITG Workshop on Smart Antennas (WSA)*, 2021, pp. 1–6.
- [10] E. Balevi, A. Doshi, A. Jalal, A. Dimakis, and J. G. Andrews, "High dimensional channel estimation using deep generative networks," *IEEE J. Sel. Areas Commun.*, vol. 39, no. 1, pp. 18–30, 2021.
- [11] A. Vaswani, N. Shazeer, N. Parmar, J. Uszkoreit, L. Jones, A. N. Gomez, L. Kaiser, and I. Polosukhin, "Attention is all you need," *arXiv preprint arXiv:1706.03762*, 2017.
- [12] J. Li, R. Wang, Y. Yuan, W. Zheng, B. He, and M. Li, "Wireless channel estimation based on transformer and super-resolution," 2023.
- [13] D. Luan and J. S. Thompson, "Channelformer: Attention based neural solution for wireless channel estimation and effective online training," *IEEE Trans. Wireless Commun.*, vol. 22, no. 10, pp. 6562–6577, 2023.
- [14] V. Nair and G. E. Hinton, "Rectified linear units improve restricted boltzmann machines," in *Proceedings of the International Conference on Machine Learning (ICML)*, 2010, pp. 807–814.
- [15] Y. LeCun, L. Bottou, G. B. Orr, and K. R. Müller, "Efficient backprop," in *Neural Networks: Tricks of the Trade*. Springer, 2012, pp. 9–48.
- [16] D. A. Clevert, T. Unterthiner, and S. Hochreiter, "Fast and accurate deep network learning by exponential linear units (ELUs)," *arXiv preprint arXiv:1511.07289*, 2015.
- [17] D. Scherer, A. Müller, and S. Behnke, "Evaluation of pooling operations in convolutional architectures for object recognition," in *Artificial Neural Networks—ICANN 2010*. Springer, 2010, pp. 92–101.
- [18] I. Greenberg, N. Yannay, and S. Mannor, "Optimization or architecture: How to hack Kalman filtering," in *Proc. of the Int. Conf. on Neural Information Processing Systems (NeurIPS)*, 2023.
- [19] L. V. Nguyen, N. T. Nguyen, N. H. Tran, M. Juntti, A. L. Swindlehurst, and D. H. N. Nguyen, "Leveraging deep neural networks for massive MIMO data detection," *IEEE Wireless Commun.*, vol. 30, no. 1, pp. 174–180, 2023.
- [20] N. Shlezinger and Y. C. Eldar, "Model-based deep learning," *Foundations and Trends® in Signal Processing*, vol. 17, no. 4, pp. 291–416, 2023.
- [21] G. Revach, N. Shlezinger, X. Ni, A. L. Escoriza, R. J. G. van Sloun, and Y. C. Eldar, "KalmanNet: Neural network aided kalman filtering for partially known dynamics," *IEEE Trans. Signal Process.*, vol. 70, pp. 1532–1547, 2022.
- [22] S. Hochreiter and J. Schmidhuber, "Long short-term memory," *Neural Computation*, vol. 9, no. 8, pp. 1735–1780, 1997.
- [23] K. Cho, B. van Merriënboer, C. Gulcehre, D. Bahdanau, F. Bougares, H. Schwenk, and Y. Bengio, "Learning phrase representations using RNN encoder–decoder for statistical machine translation," in *Proc. the Conference on Empirical Methods in Natural Language Process. (EMNLP)*, Oct. 2014, pp. 1724–1734.
- [24] G. Welch and G. Bishop, "An introduction to the Kalman filter," University of North Carolina at Chapel Hill, USA, Tech. Rep., 1995.
- [25] G. Choi, J. Park, N. Shlezinger, Y. C. Eldar, and N. Lee, "Split-KalmanNet: A robust model-based deep learning approach for state estimation," *IEEE Trans. Veh. Technol.*, vol. 72, no. 9, pp. 12326–12331, 2023.
- [26] S. Shen, J. Chen, G. Yu, Z. Zhai, and P. Han, "Kalmanformer: Using transformer to model the kalman gain in kalman filters," *Frontiers in Neuroinformatics*, vol. 18, p. 1460255, 2025.
- [27] N. Shlezinger, G. Revach, A. Ghosh, S. Chatterjee, S. Tang, T. Imbiriba, J. Dunik, O. Straka, P. Closas, and Y. C. Eldar, "Artificial intelligence-aided Kalman filters: AI-augmented designs for Kalman-type algorithms," *IEEE Signal Process. Mag.*, vol. 42, no. 3, pp. 52–76, 2025.
- [28] C. Jung, T. Ha, H. Kim, and J. Park, "State estimation with 1-bit observations and imperfect models: Bussgang meets Kalman in neural networks," 2025. [Online]. Available: <https://arxiv.org/abs/2507.17284>
- [29] Q. Xu, J. Sun, and Z. Xu, "Efficient MU-MIMO beamforming based on majorization-minimization and deep unfolding," *IEEE Trans. Wireless Commun.*, pp. 1–1, 2025.
- [30] M. Khani, M. Alizadeh, J. Hoydis, and P. Fleming, "Adaptive neural signal detection for massive MIMO," *IEEE Trans. Wireless Commun.*, vol. 19, no. 8, pp. 5635–5648, 2020.
- [31] L. Liu, C. Oestges, J. Poutanen, K. Haneda, P. Vainikainen, F. Quitin, F. Tufvesson, and P. D. Doncker, "The COST 2100 MIMO channel model," *IEEE Wireless Commun.*, vol. 19, no. 6, pp. 92–99, 2012.
- [32] S. Coleri, M. Ergen, A. Puri, and A. Bahai, "Channel estimation techniques based on pilot arrangement in OFDM systems," *IEEE Trans. Broadcast.*, vol. 48, no. 3, pp. 223–229, 2002.
- [33] Y. Choi, J. H. Bae, and J. Lee, "Low-complexity 2D LMMSE channel estimation for ofdm systems," in *Proc. IEEE Veh. Technol. Conf.*, 2015, pp. 1–5.
- [34] D. P. Kingma and J. Ba, "Adam: A method for stochastic optimization," *arXiv preprint arXiv:1412.6980*, 2014.
- [35] P. J. Huber, "Robust estimation of a location parameter," *Annals of Mathematical Statistics*, vol. 35, no. 1, pp. 73–101, 1964.
- [36] 3rd Generation Partnership Project (3GPP), "NR; physical channels and modulation," 3GPP, Tech. Rep. TS 38.211, April 2025, release 18.
- [37] T. Ha, <https://github.com/TaeJun1999/Attention-aided-MMSE>.
- [38] C. Qing, W. Hu, Z. Liu, G. Ling, X. Cai, and P. Du, "Sensing-aided channel estimation in ofdm systems by leveraging communication echoes," *IEEE Internet of Things J.*, vol. 11, no. 23, pp. 38023–38039, 2024.
- [39] N. Kim, I. P. Roberts, and J. Park, "Splitting messages in the dark-Rate-splitting multiple access for FDD massive MIMO without CSI feedback," *IEEE Trans. Wireless Commun.*, vol. 24, no. 4, pp. 3320–3332, 2025.